

Soil Anchors modeled by an embedded formulation allowing slip

H. Hartl & M. Pernthaner

Institute for Structural Concrete, Graz University of Technology

ABSTRACT: A finite element formulation, which incorporates anchors by the embedded approach, is shown. Hence, the anchor can be formulated independently of the mesh nodes. Slip between the anchor and the soil is accounted for at the material level. The capability of this approach is shown in case studies. Further a constitutive model for concrete is briefly presented, which is able to account for cracking, crushing, creep & shrinkage. This concrete model in combination with the embedded reinforcement is able to simulate a realistic behavior of reinforced concrete. A diaphragm wall with three anchor layers is investigated in a case study. The results employing advanced constitutive relation for concrete are compared to those employing linear elastic material for concrete.

1 INTRODUCTION

If an anchor should be optimized in length, transfer length and inclination by means of a FE-analysis, the formulation of the anchor should be independent of the soil mesh nodes for convenience at preparing input data. In general, anchors are frequently modeled by truss elements, which are connected to the mesh nodes of the soil, either direct or a joint element may be employed for the interface. The embedded formulation presented by Elwi (1986) allows a definition of the anchors, which is independent of the mesh node location. Initially the displacement field of the parent element and of the anchor is coupled, this restriction can be relaxed at the material level, Hartl (2000a, 2000b).

Reinforced Concrete decreases stiffness significantly when the concrete cracks. The combination of the embedded approach for the reinforcement with a proper model for concrete allows a realistic simulation of reinforced concrete in the analysis. The difference of an advanced concrete model rather to a linear elastic ones is shown. Deformations and internal forces of a diaphragm wall are compared.

A existing finite element / boundary element program, *BEFE* (2001), is extended for the theory presented here, Hartl (2002). The presented examples are performed with *BEFE*, Pernthaner (2002).

2 MODELING OF ANCHORS UTILIZING THE EMBEDDED APPROACH

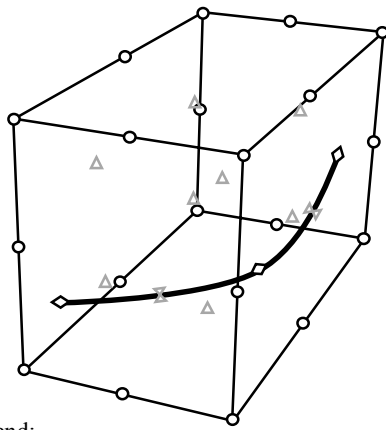
A soil anchor can be addressed as a line reinforcement of a parent material. Such a line reinforcement can be modeled by the embedded approach.

The major advantage of the embedded approach is, that the mesh of the parent domain can be prepared independently of the anchor layout. Thus, the mesh can be designed with a high regularity and a variation of anchor length or anchor inclination does not require a new mesh for the domain.

The anchor needs to be defined in global coordinates only. A preprocessing routine detects automatically the intersection of the anchor with the parent element faces as shown in Hartl (2000a).

The integration of the stiffness matrix within the finite element framework is straightforward for the parent element. It is the first term of Eq. (1). Employing the embedded approach, the reinforcement stiffness is added within the same framework. The employed approach was proposed by Elwi (1986) for the 2D case. The extension to the general 3D case is straightforward, Cheng (1993). The stiffness of the reinforcement is not homogeneous and isotropically distributed over the whole parent element, but available along the reinforcement only. Thus, integration for the reinforcement stiffness has to be performed along the rebar. We have to determine appropriate sample points for the numerical integration (Gauss points) along the reinforcement. The orientation of the reinforcement in this point must be computed, too. The crux in this method is that the integration points of the reinforcement need to be found in local coordinates of the parent elements. This inverse mapping is not straightforward, a Newton root finding algorithm in three dimensions (optimization) needs to be applied in order to find these integration points for the rebar within the parent element.

$$\mathbf{K}^e = \int_{parent} \mathbf{B}^{eT} \mathbf{D}_c \mathbf{B}^e \cdot dV + \int_{rebar} \mathbf{B}^{eT} \mathbf{T}_{\varepsilon,gl}^T \mathbf{D}_r \mathbf{T}_{\varepsilon,gl} \mathbf{B}^e \cdot dV \quad (1)$$



- Legend:
- Node point of parent element (Degree of freedom)
 - ◇ Rebar point (not a DOF)
 - △ Integration point for the parent element
 - × Integration point for the rebar

Figure 1 Parent element with embedded reinforcement

Figure 1 shows that the reinforcement is neither restricted to the parent element nodes nor it needs to be parallel to the element boundaries. It can start at any point within the parent element and it can follow a curved path as well.

3 INCORPORATION OF BOND SLIP

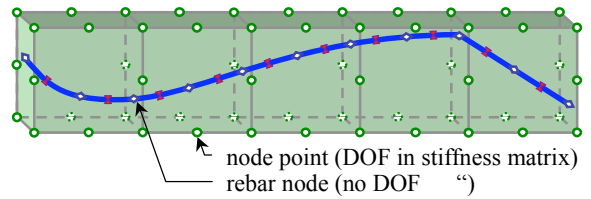
The displacement field of the parent element applies for the rebar within the embedded approach as well. Thus, perfect bond is obtained. If the slip between the anchor and the soil should be accounted for, this restriction to perfect bond needs to be relaxed.

One way is to introduce slip degrees of freedom between the parent element and the rebar. Therefore, the finite element program must offer a way to add user defined elements, since the size of the element stiffness matrix rises. Such an approach is shown in very detail in Hartl (2002).

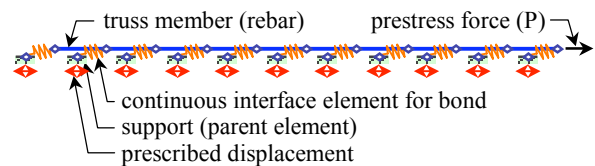
3.1 Supplementary Interface Model

Another way is to account for bond slip by introducing interface elements on the material level after the nodal deformations are computed by the global stiffness matrix. The concept of this so called "supplementary interface model" is shown in Figure 2. The reinforcement is embedded in a classical way without a slip degree of freedom into the parent elements (Figure 2a). Hence, the global analysis computes a deformation of the domain, which assumes perfect bond for the reinforcement. On the material level, this perfect bond situation is relaxed by connecting the reinforcement to the parent elements via continuous interface elements. This is illustrated by a truss analogue (Figure 2b). The truss members are the reinforcement, the supports are represented by the parent elements. The truss elements are connected to the parent elements via bond springs, which are modeled as continuous interface elements. Yet, the strain field of the domain is integrated along the reinforcement path. The deformation of the parent element is applied as support displacement in the truss model. A prestress

force can be applied at the truss nodes, Hartl (2000b). The difference in reinforcement forces computed along the truss analogue compared to forces assuming rigid bond, are mapped back as residual nodal forces of the parent element.



a) Situation in the domain



b) Truss model at the material level

Figure 2 Illustration of the supplementary interface model

This formulation of embedded rebars allowing slip can be employed equally for soil anchors and for rebars/tendons in concrete members. Thus, once a proper material law for concrete is employed, soil structure interaction problems can be studied, where nonlinear phenomenon of the soil and of reinforced concrete is taken into account.

3.2 Input for the Supplementary Interface Model

An anchor can be embedded in the parent element mesh as shown in Figure 6. The initial anchor force needs to be provided in that load case in which the anchor gets installed. An optional wedge-pull-in, which is applied in the subsequent load case, may be provided additionally.

3.2.1 Input of the anchor

The input of the anchor geometry is simple, only following input about the anchor-geometry needs to be provided.

- start point coordinates of the anchor and the anchor cross section area
- start point coordinates of the transfer length and the grout body cross section diameter
- end point coordinates of the anchor

The program detects the intersection points with the parent element mesh automatically. Additionally, the cross sectional area, Young's modulus and the yield limit of the anchor need to be provided.

3.2.2 Input of the interface

The constitutive model for an interface needs to be provided as a bond stress - slip diagram. Slip is the relative displacement between a certain node at the anchor and the associated node in the soil. Two constitutive models are available in the program for the interface between the reinforcement and the parent material. One is the well-known Mohr-Coulomb

model, the other one is a more general slip formulation.

3.2.2.1 Mohr-Coulomb interface model

Figure 3 shows the classical Mohr-Coulomb model for frictional situations. The overburden stress can be accounted for automatically. Once the peak shear stress is reached, the shear stress is assumed to remain constant with increasing slip. No residual shear stress branch is considered.

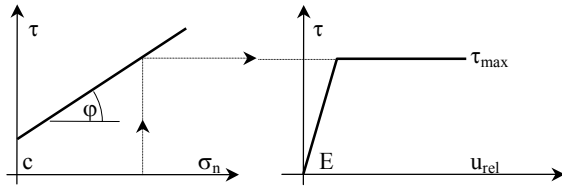


Figure 3 Mohr-Coulomb model for the anchor-soil interface

3.2.2.2 Model Code 90 interface model

Figure 4 shows the generic shape for of the bond stress - slip relation given in Model Code 90 (1993) for rebars embedded in concrete. The model has a nonlinear ascending branch (until s_1), an optional plateau ($s_1 \div s_2$) at the peak shear stress (τ_{max}), a descending branch ($s_2 \div s_3$) and a residual branch (τ_{res}) from s_3 on. This model can be adopted for numerous interface situations.

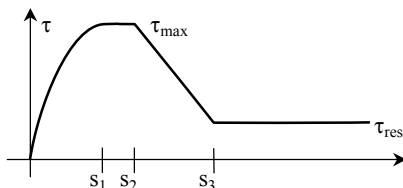


Figure 4 Bond stress - slip diagram acc. to Model Code 90

4 CAPABILITY OF THE SLIP FORMULATION - CASE STUDY OF A PULL OUT ANALYSIS

4.1 Investigated example

The basis of the following section is a benchmark example of the DGGT, Schweiger (2000). Figure 5 shows the investigated deep excavation with a diaphragm wall and three anchor layers.

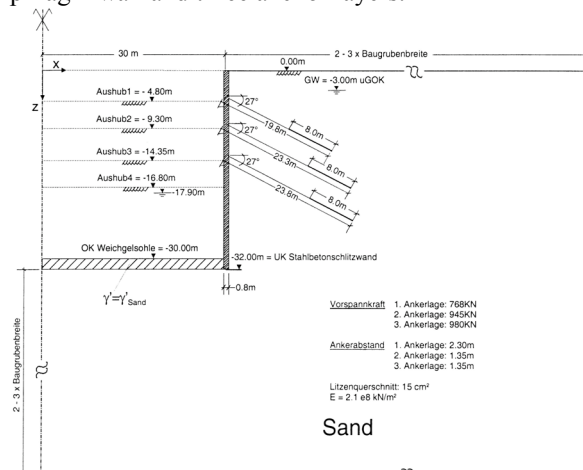


Figure 5 Geometry and excavation, Schweiger (2000)

Figure 6 shows a detail of the employed mesh for the analysis with BEFE carried out by Pernthaler (2002). All elements are quadrilateral and have parabolic shape functions. This mesh is referred in the following sections as standard mesh. A refined mesh with improved aspect ratios and about 5 times as much elements got generated for verification purposes.

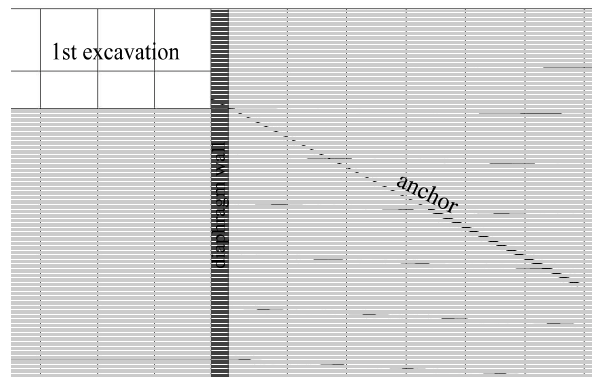


Figure 6 Mesh-detail around the first embedded anchor

4.2 Anchor embedded in very stiff soil (rock)

In this case the soil is assumed to behave like rock material by setting the Young's modulus and the cohesion to high values. Two different types for the interface got investigated as shown in Figure 7. Interface type A is assumed to behave like a rebar-concrete interface does. It has a very stiff nonlinear ascending branch and a short plateau before it decreases to the residual strength. Interface type B coincides with interface type B in section 4.3 and is described there in detail. A diameter of 17cm is assumed for the grout-body cross section.

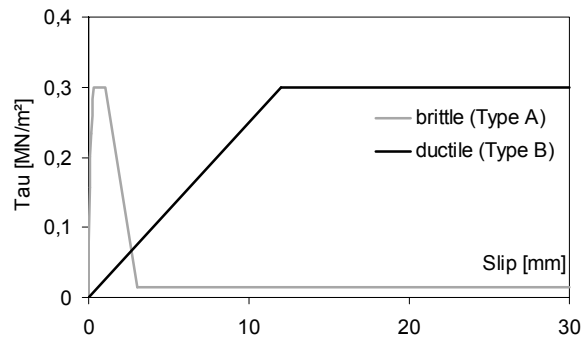


Figure 7 Interface type A and type B

The performance of the anchor-force, anchor-slip and the activated bond-stress due to slip is shown in Figure 8. The anchor force decays in the transfer length dependent on the interface spring stiffness. The highest anchor slip can be observed at the wall and it decreases linearly along the anchor until the transfer length is reached, then the slip decays due to the effect of the bond springs. The activated bond stress shows for an anchor force of 600kN and interface type A, that the residual branch of the bond stress - slip relation is reached at the beginning of the grout-body. The ultimate force for interface type A is 600kN due to the rather brittle interface while the ultimate force is 1280kN for the ductile interface (type B).

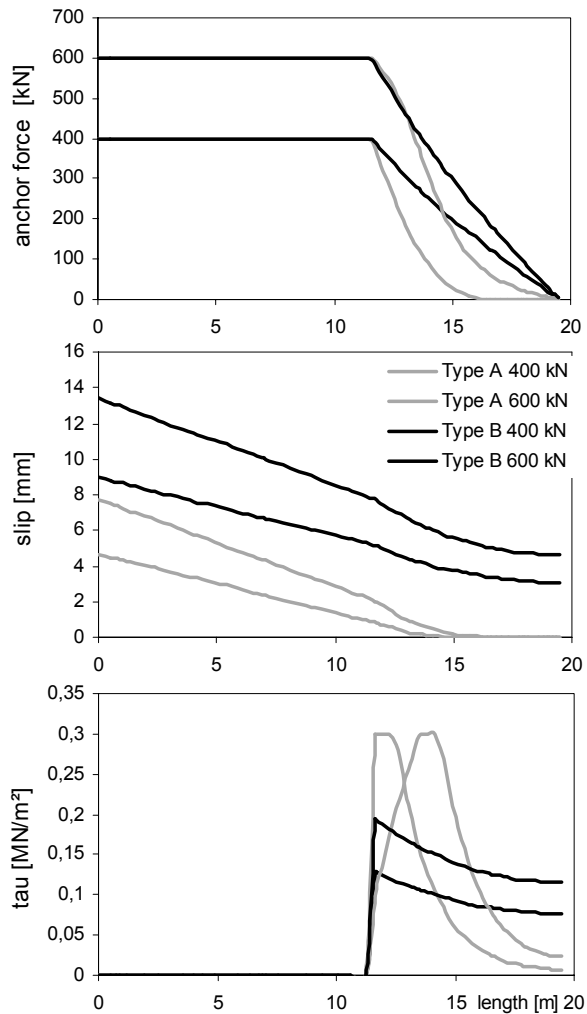


Figure 8 Anchor-force, anchor-slip & bond-stress

4.3 Anchor embedded in sand

In this case the soil is assumed to behave as described in Schweiger (2000). Two different types for the interface got investigated as shown in Figure 9. Interface type B is assumed to follow a linear ascending branch up to a peak shear stress, which is three times the overburden stress times the friction coefficient. This assumption is in accordance with recommendations given in Smolczyk (1991). It is assumed to behave infinite ductile after the peak shear stress is reached. A diameter of 17cm is assumed for the grout-body cross section. Interface type C decreases the shear stress with increasing slip after peak shear stress is reached. The residual shear stress is assumed to be 85% of the overburden stress times the friction coefficient.

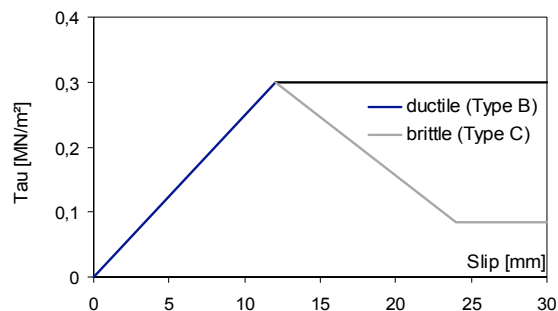


Figure 9 Interface type B and type C

The slip diagram in Figure 10 has a remarkable form. The slip behind the diaphragm wall increases along the anchor in the soil. This is due to the enormous deformation in the soil just behind the wall, especially due to the deformation component in the vertical direction. A significant increase in slip can be observed as well at the anchor short before the grout-body starts. The transfer-body pushes into the soil, thus the sudden increase of slip. These trends can be observed at the standard mesh and at the refined mesh. However, both effects may be numerically as well, since the big deformations behind the wall, especially the vertical ones are a Mohr-Coulomb effect. And no enhanced soil parameters are considered for the elements nearby the grout-body. It is also remarkable, that the slip increases again at the end of the transfer length. The transfer-section is pulled towards the anchor and triaxial tension is the consequence on the end of the grout-body. Hence, the soil trends to move to the opposite direction than the anchor in this specific region.

The bond stress diagram follows out of the slip diagram. The bond stress diagram shows for interface type C and 1000kN anchor force at the beginning of the transfer length a low bond stress since the peak stress is exceeded and the residual branch is reached. The maximum anchor force is for interface type C 1000kN, while a maximum anchor force of 1280kN can be activated by the more ductile interface type B.

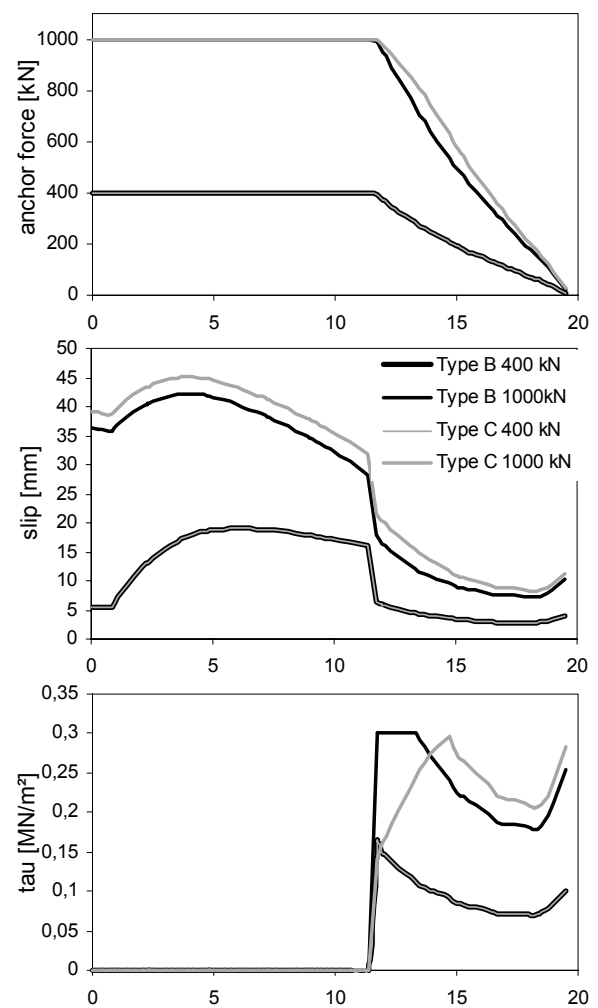


Figure 10 Anchor-force, anchor-slip & bond-stress

5 NONLINEAR EFFECTS OF THE REINFORCED CONCRETE

It is well known that stiffness of cracked concrete is significantly lower compared to stiffness of uncracked concrete. Figure 11 shows the stiffness of a concrete cross section on the ordinate and the applied moment on the abscissa. For an insignificant load increase, the stiffness of the concrete will decrease tremendously due to cracking. The dashed line in Figure 11 shows the limit of the service load. It is the design load without any safety factor. The service load is for sparsely reinforced sections just slightly higher compared to this moment, which causes cracking. The concrete sections used for geotechnical applications are normally big and the reinforcement ratio is usually low. Hence, the concrete may follow a cracked performance as likely as an uncracked performance.

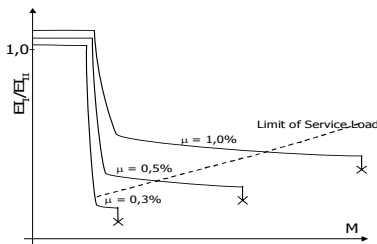


Figure 11 Stiffness - moment diagram

The right stiffness for each integration point of the concrete can be accounted for in *BEFE* by employing a proper constitutive model for concrete. Crushing due to compression overload is accounted for by the Ottosen yield surface, Ottosen (1976).

A rotating crack model accounts for tensile failure of concrete. The tensile behavior of concrete for specimens with different length is shown in Figure 12. The left diagram is a stress - strain diagram and the right one is a stress - elongation diagram. Where the pre-peak behavior is independent of the specimen length, is the softening behavior dependent on the specimen length.

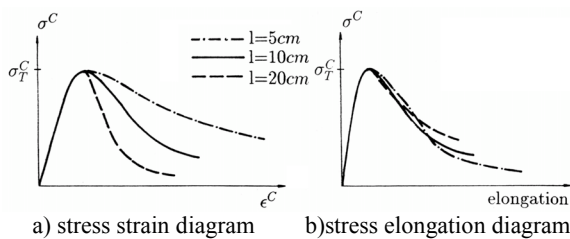


Figure 12 Tensile behavior of concrete

A fictitious crack model, originally proposed by Hillerborg (1976), is introduced in order to obtain results, which are independent of the element size. The pre-peak behavior and tensile yielding is formulated in a stress strain diagram. The softening regime is formulated in a stress elongation diagram, which is controlled by the crack energy and the length associated to an integrated point, compare Figure 13. In a 3D analysis the three principal stresses can be related separately to this model, since there is only little interaction of concrete tensile stresses. The model is re-

ferred to as rotating crack model, it can be employed as an isotropic or as an anisotropic crack model.

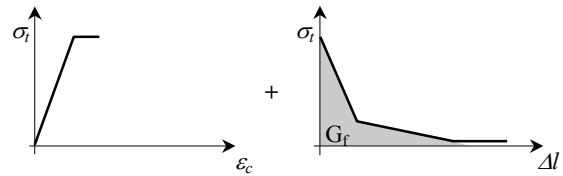


Figure 13 Modeling of the tensile behavior of concrete

5.1 Case study of a diaphragm wall

The diaphragm wall given in Figure 5 is investigated. Assuming a linear elastic diaphragm wall the highest bending moment occurs after the third excavation is performed and before the third anchor layer is installed. The moment is 700kNm, the according normal force is 200kN. A conventional design requires 30cm²/m reinforcement, which is installed for practical reasons on both sides. The minimum reinforcement is 16cm².

The FE-analysis performed here is in the terminology of structural engineering a serviceability analysis since characteristic material parameters enter the analysis. In such a case steel stress should not exceed 300 ÷ 350MN/m². Figure 14 shows that steel stress is about half of the allowed limit for A_s = 30cm²/m. Even if only the minimum reinforcement for such a cross section (16cm²/m) is provided, the steel stress raises only to 200MN/m². The diaphragm wall remains stable albeit less than the minimum reinforcement is provided. However, this is disregarded by concrete design codes and even in the analysis is a nearly unreinforced wall not stable any more.

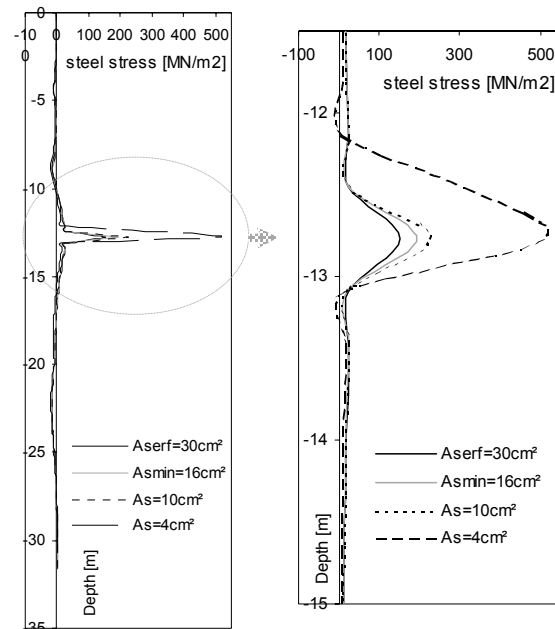


Figure 14 Steel stress of reinforcement in diaphragm wall

Figure 15 shows the deformation in the load case of the highest bending moment (after the third excavation and before the third anchor layer). Decreasing the amount of reinforcement increases the deformation in the region of the high moment and a continuously growing kink develops. It can be seen that a weak re-

gion does not endanger the entire wall. A redistribution of forces occurs and the moment is reduced.

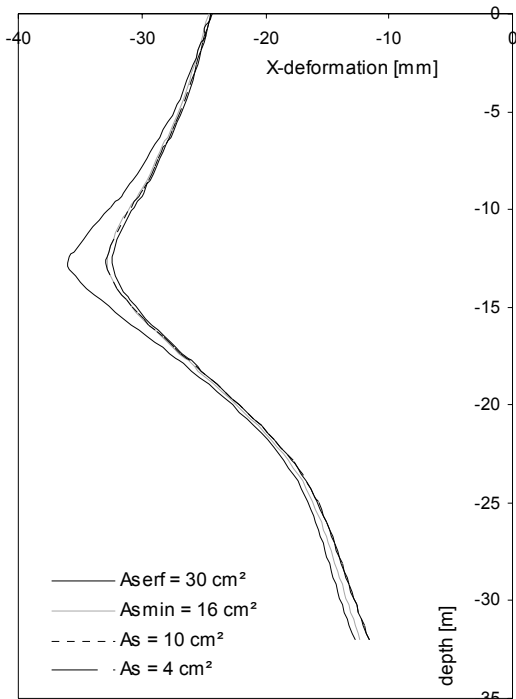


Figure 15 Deformation dependent of the reinforcement

Figure 16 shows the deformation at the head of the diaphragm wall over all load cases (starting at lowering the ground water table and all sequences of excavations and installment of anchors). It can be seen that the head deformation depends only little on the provided reinforcement.

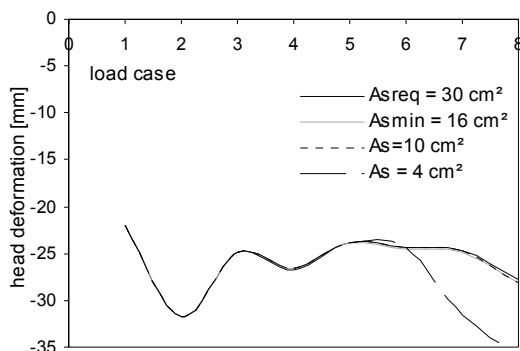


Figure 16 Deformation at the head of the diaphragm wall

6 CONCLUSION

It is shown that an embedded formulation of reinforcement is equally appropriate for tendons in concrete as for anchors in soil. The presented results are reasonable, and the performance of the anchors is in accordance with the generic shapes provided in Blümel (1996).

In section 5.1 are different reinforcement ratios of a diaphragm wall investigated. The reinforcement starts with the amount, which is obtained by a design based on the moment obtained by introducing an elastic wall in the FE-analysis. In this case, where a structural indeterminate system is investigated a reduction to the minimum reinforcement can be done without endangering the wall. Even a further reduction of reinforcement could be done in the considered

case. However, a reduction of reinforcement to an amount, which is lower than the minimum reinforcement defined by design codes, is highly disregarded since a brittle failure of the diaphragm wall may occur.

REFENERNCE

- Beer G. (2001). "BEFE user's, reference & verification manual", CSS, Graz, 2001
- Blümel M. (1996). "Untersuchungen zum Tragverhalten vollvermörtelter Felsbolzen im druckhaften Gebirge", Dissertation, Graz University of Technology, 1996
- CEB-FIP 1993. Comité Euro-International du Béton, "CEB-FIP Model Code 1990", London, Thomas Telford, 1993
- Cheng Y.M., Fan Y. 1993. "Modeling of reinforcement in concrete and reinforcement confinement coefficient", Finite Elements in Analysis and Design, Elsevier, 1993, 13, pp. 271-284
- Elwi A.E., Hruday T.M. 1989. "Finite Element Model for Curved Embedded Reinforcement", Journal of Engineering Mechanics, ASCE, April 1989, 115(4), pp. 740-754
- Hartl H., Sparowitz L, Elgamal A. 2000a. "The 3D computational Modeling of Reinforced and Prestressed Concrete Structures", Bergmeister K. (ed.), Proceedings of the 3rd International PhD Symposium in Civil Engineering, Vienna, 2000, vol. 2, pp 69-79
- Hartl H., Elgamal A. 2000b, "Nicht lineare kontinuumsmechanische Modellierung vorgespannter Konstruktionen (Non Linear Modeling of Prestressed Structures based on a Continuum Mechanics Approach)" (in English), Heft 45 / September 2000, Österreichische Vereinigung für Beton- und Bautechnik, Vienna, pp. 87-96
- Hartl H. 2002. "Development of a 3D Finite Element Tool based on Continuum Mechanics for Reinforced Concrete Structures and its Application to Soil Structure Interaction", Doctoral Thesis, Graz University of Technology, 2002 (in prep.)
- Hillerborg A., Modéer M., Peterson P.E. 1976. "Analysis of Crack Formation and Crack Growth in Concrete by Means of Fracture Mechanics and Finite Elements", Cement and Concrete Research, 6, 1976, pp 773-782
- Pernthaner M., (2002). "Interaktion von Schlitzwand und nahen Bauwerken unter Einbeziehung der Nichtlinearität der Betonkonstruktionen", Diploma Thesis, TU-Graz, 2002 (in prep.)
- Schweiger H.F., (2000). "Ergebnisse des Berechnungsbeispiels Nr. 3 "3-fach verankerte Baugrube"", Tagungsband Workshop "Verformungsprognose für tiefe Baugruben", Stuttgart, 16. and 17.3.2000, 7-67
- Smolczyk U., (1991). "Grundbau - Taschenbuch", Ernst& Sohn, Berlin, 1991